RSC Advances

PAPER

View Article Online
View Journal | View Issue

Cite this: *RSC Adv.*, 2021, **11**, 19387

Magnetic GO/Fe_3O_4 for rapid malachite green (MG) removal from aqueous solutions: a reversible adsorption†

Wenwen Li,[ab] Miaoqing Xu,[a] Qian Cao,[a] Jie Luo,[a] Shiyong Yang *[ab] and Guangchao Zhao *[a]

Magnetic GO/Fe_3O_4 was synthesized using co-precipitation of Fe^{2+} and Fe^{3+} composited with graphene oxide (GO) in alkaline conditions. SEM, XPS, FTIR, N_2 adsorption and VSM techniques were employed to characterize the surface peculiarities of GO/Fe_3O_4 and it was then used for removal of malachite green (MG). The key influencing factors on adsorption, such as mass ratio of GO, pH value and dosage of GO/Fe_3O_4, were investigated. The Freundlich isotherm was well fitted to the experimental data, suggesting GO/Fe_3O_4 has more than one type of reactive site. By comparing the adsorption of anionic dyes and cationic dyes onto GO/Fe_3O_4, it was concluded that GO/Fe_3O_4 could be extensively applied to take up cationic dyes mainly for electrostatic interaction. In addition, the spent GO/Fe_3O_4 was almost 100% recovered in a water bath at 80 °C. An ultraviolet-visible (UV-vis) spectrophotometer and an atom adsorption spectrophotometer (AAS) were used to determine leached GO and Fe ions discharged into the treated solutions. Low leaching showed that magnetic GO/Fe_3O_4 is a stable environmentally-friendly material.

Received 19th March 2021
Accepted 11th May 2021

DOI: 10.1039/d1ra02209a

rsc.li/rsc-advances

1. Introduction

Malachite green (MG) is a toxic organic chemical that has been widely used to control fish parasites and disease.[1,2] It is also used as a staining agent in ceramics, textiles, leather, food and histochemical studies[3,4] due to its low cost.[5] Its long-term application and hard-to-degrade nature led to its accumulation in aquatic environments that eventually endangered human health and environmental safety.

There is therefore an urgent mission to find appropriate approaches to reduce the environmental risks, and to inactivate or to remove hazardous substances[6–8] from the environment. At present, a variety of means, including photo-degradation,[9] catalysis,[10,11] the Fenton reaction,[12] phyto-degradation[13] and adsorption,[14–16] have all been used for such purposes. Among these approaches, adsorption is one of the most widely accepted techniques because of its environmental compatibility and operability. High adsorption efficiency generally depends on the affinity of functional groups on the surface of the adsorbent to targets.[17] A number of materials, including nanoparticles of metal oxide,[18] organically modified mineral substances,[19,20] biochar,[21] and aerogel,[22] have been successfully employed to remove MG.

Graphene oxide (GO) is a novel carbon-based material that has a single atom layer of sp^2-hybridized carbon arranged in a honeycomb-like structure and its functional groups include hydroxyl, carboxyl, and epoxy groups.[23–25] Compared to other carbon-containing adsorbents, the graphene family[26] has an improved potential for the adsorption of hazardous metal ions,[27–29] cationic dyes[30–32] and aromatic compounds[33,34] from aqueous solutions. But unitary nano-scale GO is difficult to isolate by filtration and centrifugation.

In contrast, magnetic material could realize magnetic separation independent of other driving forces.[35] Coincidently, GO combined with magnetic nano-Fe_3O_4 is of great interest because it has been proved to be an ideal adsorbent to remove organic dyes and inorganic metal ions. The electrons of benzene rings on GO sheets contribute to possible donor–acceptor interaction, electrostatic attraction, chelation, and catalytic degradation.[36] In addition, magnetic GO/Fe_3O_4 could inhibit the agglomeration of graphene oxide.[37] Nevertheless, it has rarely been reported whether GO composites could be recovered or would be left over in aqueous solutions.

In this study, binary magnetic GO/Fe_3O_4 was prepared using a modified precipitation method and then its potential and efficiency as an adsorbent to eliminate MG from solutions were assayed. The results showed that the efficiency for MG adsorption increased significantly with increasing GO ratios in the composites. Also, rapid adsorption at high solution pH value

[a]School of Ecology and Environment, Anhui Normal University, Wuhu 241002, PR China. E-mail: gczhao@ahnu.edu.cn; shiyan@ahnu.edu.cn

[b]Collaborative Innovation Center of Recovery and Reconstruction of Degraded Ecosystem in Wanjiang Basin Co-founded by Anhui Province and Ministry of Education, Wuhu, Anhui 241002, PR China

† Electronic supplementary information (ESI) available. See DOI: 10.1039/d1ra02209a

suggested that electrostatic interaction is probably the preliminary adsorption force. Most important of all, GO/Fe_3O_4 can be recovered, suggesting reversible adsorption, less Fe or GO leaching and low secondary environmental pollution. Thus, GO/Fe_3O_4 is an environmentally friendly material for the removal of organic pollutants from an aquatic environment.

2. Materials and methods

2.1 Materials

MG powder was purchased from Tianjin Chemagent Research Co., Ltd (China). $FeSO_4 \cdot 7H_2O$ and $FeCl_3 \cdot 6H_2O$ were obtained from Sinopharm Chemical Reagent Co., Ltd (China). Ammonia was obtained from Shanghai Lingfeng Chemical Reagent Co., Ltd (China). Ammonium nitrate, hydrochloric acid and sodium hydroxide were purchased from Shanghai Chemical Reagent No. 1 Co., Ltd (China). GO powder was synthesized in our laboratory using a modified Hummers' method.[38] An iron magnet (70 mm long, 50 mm high and 11 mm wide) was purchased from Yongxin Magnetic Industry Co., Ltd (China). All chemicals were of analytical grade and double-distilled water was used throughout the experiments.

2.2 Synthesis of GO/Fe_3O_4 magnetic composite

GO[39] was dispersed ultrasonically in distilled water for 20 min, and then adjusted to a concentration of 1.00 mg mL^{-1}. 10.0 g of ammonium nitrate was dissolved in 20.0 mL of water, and then mixed with 20.0 mL of ammonia. The mixture was transferred to a 250 mL volumetric flask as the basic buffer solution (pH 9.5).

0, 0.2, 1.0, and 2.0 mL of GO suspension as well as 10 mL of the above-mentioned buffer solution were added to 100 mL beakers. The mixture was churned constantly while being heated to 60 °C in the presence of N_2. 0.5 mL of 5 M ammonia and a 0.5 mL mixture of 1 M $FeSO_4$ and 1 M $FeCl_3$ were simultaneously added dropwise. Half an hour later, the aqueous phase was decanted magnetically, while the black precipitates (GO/Fe_3O_4) were collected, washed using water and ethanol, and then dried at 90 °C for 24 h.

2.3 Instruments and tools

The magnetic behavior was analyzed using a Lake Shore 7404 Vibrating Sample Magnetometer VSM (Lake Shore, USA). The chemical nature of GO/Fe_3O_4 was characterized using X-ray photoelectron spectra (XPS) with a Nexsa spectrometer (Thermo Fisher, USA) equipped with an Al Kα monochromated X-ray source. The morphology of the adsorbent was characterized with S-4800 FESEM Scanning Electron Microscope images (Hitachi, Japan). An FTIR-8400S instrument (Shimadzu, Japan) was used to analyze the structure and surface groups of the material. N_2 adsorption–desorption isotherms were evaluated at 77 K to find the specific surface area and pore size distribution using ASAP 2020 PLUS (Micromeritics, USA). UV-vis adsorption spectra for dyes and GO solutions were recorded using a UV-1901 spectrophotometer (Puxi Company, Beijing).

2.4 Adsorption experiments

The effects of GO proportions, pH value (adjusted with 0.1 M HCl and 0.1 M NaOH solutions) and kinetics on adsorption were evaluated using dynamic experiments at room temperature. 100 mL (9.0 mg L^{-1} and 18 mg L^{-1}) of MG solution was transferred to a 250 mL beaker. 20 mg of the adsorbent was added and then shaken in a water-bath vibrator at 298 K and 200 rpm. 5 mL of supernatant were sampled at definite time intervals for detection.

The effects of dosage and adsorption isotherm were studied in batch experiments. GO/Fe_3O_4 (0.2–16 mg) was suspended in 100 mL triangular flasks containing 50 mL of different concentrations of MG (9.0 to 50 mg L^{-1}) and then shaken in a water-bath vibrator at 200 rpm. 200 min later, 10 mL of the solution was sampled at 200 min for detection. The concentration of MG in solution was determined spectrophotometrically at 618 nm. To ensure reproducibility and accuracy, measurements were made in at least triplicate. MG adsorption capacity (q) was calculated using the following eqn (1):

$$q_i = (C_0 - C_i)V/m \quad (1)$$

where m and V are the mass of the adsorbent and the volume of MG solution, respectively; q_i is the adsorption capacity at time t (q_t) or at equilibrium (q_e); C_0 is the initial concentration of MG and C_i is the concentration of MG at time t (C_t) or at equilibrium (C_e).

2.5 Desorption and re-adsorption experiments

The spent GO/Fe_3O_4 was thermally desorbed using a batch desorption procedure. In brief, GO/Fe_3O_4 was suspended in a flask containing 250 mL of H_2O, then the flask was arranged in a water-bath vibrator at 60 °C, 70 °C, 75 °C, 80 °C, 85 °C and 90 °C, respectively. Subsequently, the solution was magnetically decanted and the sample concentration (C_{de}) was determined.

Re-adsorption experiments followed the procedure of thermal desorption experiments. The desorbed GO/Fe_3O_4 was maintained in flasks containing MG at the same concentration and the flasks were shaken in a 30 °C water-bath vibrator at 200 rpm. A fraction of supernatant was sampled and determined at equilibrium as $C_{e,re}$.

The amounts of desorption (Q_{de}, mg g^{-1}) and re-adsorption (Q_{re}, mg g^{-1}) are determined following eqn (2) and (3), respectively:

$$Q_{de} = \frac{C_{de}\ V}{m} \quad (2)$$

$$Q_{re} = \frac{(C_0 - C_{e,re})V}{m} \quad (3)$$

where C_{de} is the MG concentration after desorption (mg L^{-1}); C_0 is the initial concentration (mg L^{-1}) of MG and $C_{e,re}$ is the concentration of MG after re-adsorption (mg L^{-1}); m is the mass of the spent GO/Fe_3O_4 (g), and V is the total volume of the MG solution (L) and is set to be constant in the adsorption, desorption and re-adsorption process.

3. Results and discussion

The magnetic GO/Fe_3O_4 was synthesized through a classical co-precipitation procedure. Under alkaline conditions, GO could be well dispersed to form exfoliated sheets with a large number of oxygen-containing functional groups present on the GO

surface. When Fe^{2+}/Fe^{3+} ions were added dropwise, they were rapidly deposited onto the negative GO layers through electrostatic interaction and possibly through chelation. Thus, the black precipitates tightly attached on GO sheets gradually formed multidimensional structures.[40]

3.1 Characterization of GO/Fe_3O_4

Fig. 1A depicts two types of shapes in the SEM image of GO/Fe_3O_4 at a 2 μm scale. On the one hand, Fe_3O_4 agglomerates at an average particle size of 50 nm; see also Fig. S1.† Meanwhile, GO forms thin sheets with a few layers and attaches to Fe_3O_4, resulting in wrinkled structures. The outer sheet of the wrinkled structures of GO becomes ridged and covers Fe_3O_4 nanoparticles. As a result, its three-dimensional structure is beneficial for adsorption due to its increased surface area.[41] It is also possible that the metallic nanoparticles have supplied stable platforms for GO.[42,43] Therefore, GO/Fe_3O_4 is a powerful material for cyclic utilization.

The XPS survey spectrum is shown in Fig. 1B, which is highly consistent with Chong's XPS spectrum of Fe^0/Fe_3O_4/graphene.[44] The binding energies at 711 eV and 724 eV could be ascribed to Fe^{2+} and Fe^{3+}, respectively. The results may demonstrate the presence of Fe_3O_4 nanoparticles. C–C and C–O groups in the GO surface have contributed the main parts to the C 1s peak and O^{2-} to O 1s. The observed ratio of O/C was very high, indicating the large scale of oxygen-containing groups on the surface of GO/Fe_3O_4.

In the N_2 adsorption assay, the calculated specific surface area of GO/Fe_3O_4 was 132.2 $m^2\ g^{-1}$ (in contrast, that of GO was 28.9 $m^2\ g^{-1}$) based on Brunauer–Emmett–Teller (BET) isotherm fitting (Fig. 1C). The N_2 adsorption–desorption isotherm curve belongs to the type IV isotherm model according to the International Union of Pure and Applied Chemistry (IUPAC) nomenclature. The hysteresis loop appeared at $p/p_0 = 0.4$–1.0, indicating that the capillary condensation phenomenon had taken place in the mesoporous structure existing in GO/Fe_3O_4.[44] The pore sizes of GO and GO/Fe_3O_4 measured by an

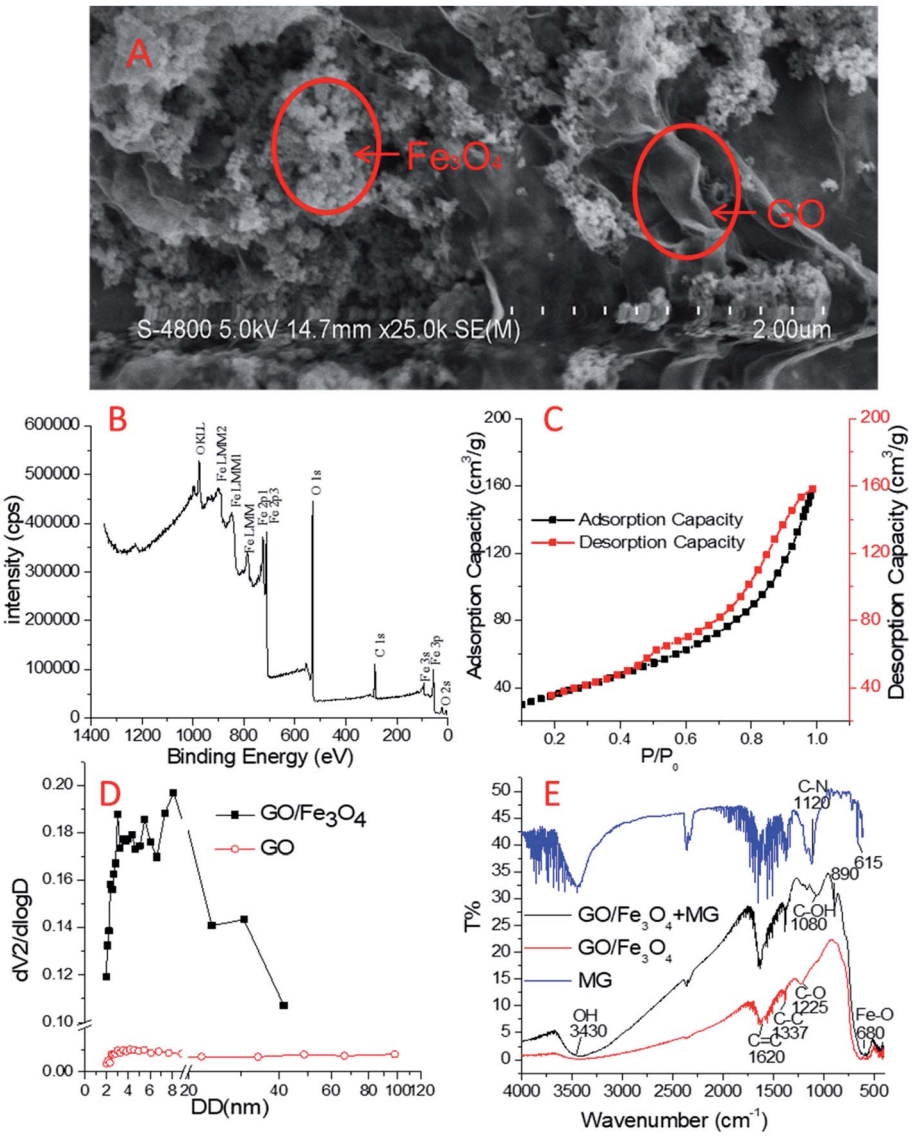

Fig. 1 The morphology of GO/Fe_3O_4 in SEM (A), X-ray photoelectron spectroscopy spectra of GO/Fe_3O_4 in the survey scan (B), N_2 adsorption–desorption isotherms for GO/Fe_3O_4 (C), pore-size distribution (D), and FTIR spectra of MG and GO/Fe_3O_4 (E).

N_2 adsorption experiment are shown in Fig. 1D. The pore sizes of GO/Fe_3O_4 ranging from 2 to 10 nm accounted for 50.04% of the total, and the total pore volume of GO/Fe_3O_4 was 0.2574 $cm^3\ g^{-1}$. In contrast, the pore sizes of GO ranged from 2 to 50 nm and the total pore volume of GO was as low as 0.012 $cm^3\ g^{-1}$, suggesting the poor pore structure in GO. The three-dimensional structure of GO/Fe_3O_4 was assumed to contribute to the mesoporous nature.

FTIR spectra were used to characterize the functional groups of GO/Fe_3O_4, as shown in Fig. 1D. There were many peaks at about 1620 cm^{-1}, 1337 cm^{-1} and 1225 cm^{-1} on GO/Fe_3O_4, which are probably related to the sp^2 skeletal vibration of C=C, C–C and C–O stretching vibrations, respectively.[46] These bands in GO/Fe_3O_4, together with those in GO, suggest the maintenance of the oxygen-containing groups and benzene rings.[44] The weak peak at 3430 cm^{-1} meaning little O–H stretching but the strong peak at 1620 cm^{-1} meaning lots of C=C on the GO/Fe_3O_4 surface showed that there was a good ratio of GO component rather than reduced graphene oxide.[45] In addition, the sharp peak of 680 cm^{-1} represents a large ratio of Fe_3O_4 component.

The magnetic properties of GO/Fe_3O_4 were measured to determine whether sufficient magnetization could enable a fast solid–liquid separation. As shown in Fig. S2,† the saturated magnetization was 54.35 emu g^{-1} and the sharp slope of the magnetization proved its superparamagnetism. In this study the solution separated from the adsorbent in the adsorption experiments was magnetically decanted thoroughly.

3.2 Batch adsorptions

3.2.1 The effect of GO proportion on GO/Fe_3O_4 preparation. In order to test the importance of GO in MG removal, different proportions of GO were used to synthesize GO/Fe_3O_4. The mass of GO/Fe_3O_4 was approximately 10.0 mg in each complete reaction experiment. So the mass ratios of GO in 0-GO/Fe_3O_4, 2-GO/Fe_3O_4, 10-GO/Fe_3O_4 and 20-GO/Fe_3O_4 were recorded as 0%, 2%, 10% and 20%, respectively. As shown in Fig. 2, the adsorption capacity increased with increasing GO content in GO/Fe_3O_4, because an increased GO fraction results in a larger surface area. When GO was absent, the adsorption capacity of 0-GO/Fe_3O_4 at equilibrium was 4.5 mg g^{-1}, while that of 2-GO/Fe_3O_4 showed a 6-fold increase. Thus, the nano-Fe_3O_4 would contribute little to MG adsorption, and the adsorptive force between MG and GO/Fe_3O_4 was produced mainly by the affinity of GO to MG. The adsorption of MG by 10-GO/Fe_3O_4 and 20-GO/Fe_3O_4 did not differ significantly, but both

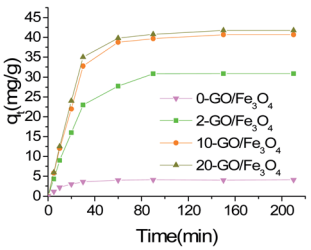

Fig. 2 Effects of GO proportion in GO/Fe_3O_4 on the adsorption of MG (MG concentration = 9 mg L^{-1}, dosage = 20 mg, temperature = 298 K, pH = 7.0).

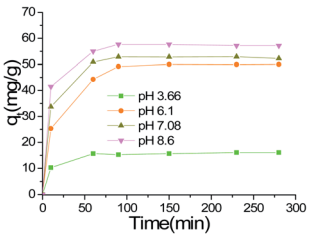

Fig. 3 Dynamic adsorption of MG onto GO/Fe_3O_4 at different pH (MG concentration = 9 mg L^{-1}, dosage = 20 mg, temperature = 298 K).

were markedly higher than that of 0-GO/Fe_3O_4. It is well known that the ideal GO is unfolded and an excessive GO content would cause a waste of resources. Therefore, 10-GO/Fe_3O_4 was chosen as the optimal GO/Fe_3O_4 for MG adsorption.

3.2.2 The effect of pH and contact time. Solution pH value is one of the most important factors that determines the adsorption property because of its effect not only on the surface charge of the adsorbent but also on the degree of ionization of the adsorbate.[47] As shown in Fig. 3, the adsorption speed and capacity of GO/Fe_3O_4 for MG decreased with decreasing pH values. This is probably related to the high concentration of H^+ that competes for cationic MG, allowing MG less opportunity to access GO/Fe_3O_4. Furthermore, the zeta potential of GO/Fe_3O_4 is pH 4.3; as a result, GO/Fe_3O_4 is positively charged when pH < 4.3 and it is negatively charged when pH > 4.3. As far as we know, MG pollution frequently happens at neutral pH, so pH 7.0 was selected for further study. Cationic MG is easily attracted to the positively charged GO/Fe_3O_4 by electrostatic attraction. The absorption capacity at pH 7.0 was found to increase to 50.5 mg g^{-1} when the contact time reached 60 min, and experimental adsorption equilibrium was almost reached at 90 min. Rapid adsorption of GO/Fe_3O_4 suggests it is a good candidate for the removal of toxic materials.

3.2.3 The effect of dosage. The adsorption spectrum of MG at different dosages of GO/Fe_3O_4 was recorded using a UV-vis spectrophotometer. As shown in Fig. 4, the results revealed that an increase in adsorbent dosage from 2 mg to 16 mg led to an absolute decrease in absorbency at 618 nm; a π–π* transition may be attributed to a triphenyl-structure at 422 nm; a π–π* transition may be attributed to single benzene structure, with absorbency at 316 nm and 250 nm; and an n–π* transition may be ascribable to N–C groups. The MG adsorption spectrum decreased with an increased dosage of GO/Fe_3O_4 without a spectral peak shift or other peaks emerging. This suggests that MG solution

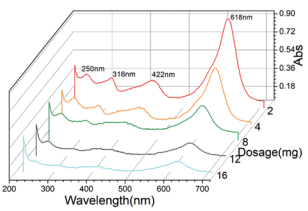

Fig. 4 UV-vis spectrum of MG solution after adsorption at different dosages of GO/Fe_3O_4 (MG concentration = 9 mg L^{-1}, temperature = 298 K, pH = 7.08, time = 200 min).

would be decontaminated rather than changing the structure of the MG molecule in solution. The observed uptake could be due to the presence of active binding sites on the large surface area of GO/Fe_3O_4. Furthermore, the effects of agitation were not significant, and the parameter of initial MG concentration is investigated in the adsorption isotherms section.

3.3 Adsorption isotherms

Freundlich and Langmuir models are widely used to fit experimental adsorption data. The Freundlich model is an empirical model based on adsorption occurring on heterogeneous surfaces. The equation is commonly described as:[48]

$$\log q_e = \log k_F + \frac{1}{n}\log c_e \quad (4)$$

where q_e is the equilibrium adsorption capacity of GO/Fe_3O_4 (mg g^{-1}), c_e represents the equilibrium concentration of MG in solution (mg L^{-1}), and k_F and n are the Freundlich constants that represent the adsorption capacity (L mg^{-1}) and adsorption strength, respectively. The magnitude of $1/n$ quantifies the favorability of adsorption and the degree of heterogeneity of the surface. $n > 1$ indicates an increase in adsorption capacity and the formation of new adsorption sites, suggesting favorable adsorption. Another widely used isotherm model is the Langmuir model, which describes monolayer and irreversible adsorption. The Langmuir model equation is given by:[49]

$$\frac{c_e}{q_e} = \frac{1}{q_{max}b} + \frac{c_e}{q_{max}} \quad (5)$$

where q_e is the equilibrium adsorption capacity of GO/Fe_3O_4 (mg g^{-1}) and c_e represents the equilibrium concentration (mg L^{-1}). q_{max} is the maximum amount of dye per unit weight of adsorbent for complete monolayer coverage and b is the Langmuir adsorption constant in L g^{-1}.

The validity of the isotherm was checked using the fitted straight lines illustrated in Fig. S3,† and the corresponding constants in different adsorption isotherms are summarized in Table 1. The high determination coefficients (R^2) suggested that the Freundlich model fitted the experimental data well. The higher K_F value at 303 K relative to that at 323 K indicated that GO/Fe_3O_4 has a higher adsorption capacity and affinity for MG. The n value between 1 and 10 represents favorable adsorption under these conditions. In conclusion, the adsorption of MG onto heterogeneous GO/Fe_3O_4 surfaces was reversible and the Freundlich isotherm also suggested that the adsorption forces may have more than one source. Although the R^2 of the Langmuir equations is lower than that of the Freundlich, the constant of q_{max} from the Langmuir equations can also be used to roughly evaluate the experimental adsorption capacity.

As shown in Table 1, almost all constants (K_F, n, q_{max}, and b) indicate that a low temperature (303 K) may facilitate the adsorption of MG onto GO/Fe_3O_4. To demonstrate the results mentioned above, the thermodynamic parameter of enthalpy (ΔH^0) was calculated using the following equation:[50]

$$\Delta H = R\frac{T_2T_1}{T_2 - T_1}\ln\frac{b_2}{b_1} \quad (6)$$

Table 1 Isothermal parameters for MG removal by GO/Fe_3O_4 at different temperatures (MG concentration = 10, 20, 30, 40, 50 mg L^{-1}, dosage = 10 mg, pH = 7.08, time = 200 min)

		Temperatures (K)	
Isotherms	Parameters	303 K	323 K
Langmuir	q_{max} (mg g^{-1})	96.9	80.8
	b (L g^{-1})	2.21	1.25
	R^2	0.988	0.971
Freundlich	K_F (L mg^{-1})	56.1	41.0
	n	3.74	3.61
	R^2	0.994	0.995

where R is the universal gas constant (8.315 J mol^{-1} K^{-1}); b is the Langmuir constant (L mg^{-1}) and T is the absolute temperature (K). A negative value $\Delta H = -2.3$ kJ mol^{-1} was calculated and indicated that the adsorption reaction is exothermic.

3.4 Adsorption kinetics

To further explore the mechanism of the adsorption process, we applied two kinetic models[37] (pseudo-first-order and pseudo-second-order) to analyze the experimental data (Fig. S4†). The pseudo-first-order kinetic equation can be expressed as eqn (7):

$$\log(q_e - q_t) = \log q_e - kt \quad (7)$$

where q_e and q_t are the adsorption capacity of MG on GO/Fe_3O_4 at equilibrium and at various times t (mg g^{-1}), respectively; k is the rate constant of the pseudo-first-order model of adsorption (min^{-1}). The pseudo-second-order model includes all the steps of adsorption, including external film diffusion and adsorption, which can be expressed as eqn (8):

$$\frac{t}{q_t} = \frac{1}{k_2q_e^2} + \frac{1}{q_e}t \quad (8)$$

where q_e and q_t are the same as those defined in the pseudo-first-order model and k_2 is the rate constant of the pseudo-second-order model of adsorption (g mg^{-1} min^{-1}).

The kinetic parameters and correlation coefficients for the removal of MG by GO/Fe_3O_4 are summarized in Table 2. The obtained maximum adsorption capacity ($q_{e,exp} = 59.0$ mg g^{-1}) is

Table 2 Adsorption kinetic parameters of MG as confirmed by the pseudo-first-order and pseudo-second-order kinetic models (initial MG concentration = 9.00, 18.0 mg L^{-1}, dosage = 20 mg, volume = 50 mL, agitation speed = 200 rpm, pH = 7.08, temperature = 303 K)

		C_0 (MG, mg L^{-1})	
Kinetic models	Parameters	9.00	18.0
Pseudo-first-order	$q_{e,cal}$ (mg g^{-1})	7.55	23.0
	k_1 (min^{-1})	0.0121	0.0112
	R^2	0.973	0.942
Pseudo-second-order	$q_{e,cal}$ (mg g^{-1})	30.3	60.0
	k_2 (g mg^{-1} min^{-1})	0.288	0.166
	R^2	0.999	0.999

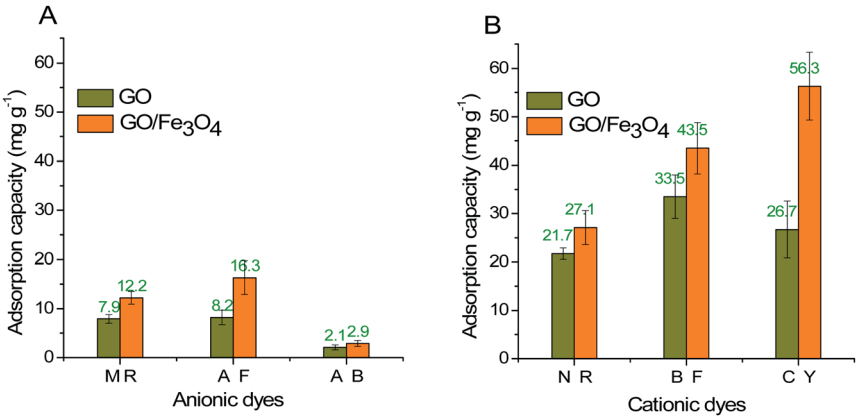

Fig. 5 The adsorption capacity of GO and GO/Fe_3O_4 for anionic dyes of Methyl Red (MR), Acid Fuchsin (AF) and Aniline Blue (AB) (A), and for cationic dyes of Neutral Red (NR), Basic Fuchsin (BF) and Crystal Violet (CV) (B).

in accordance with the calculated adsorption capacity ($q_{e,cal}$ = 60.0 mg g^{-1}) of the pseudo-second-order model. These results indicate that the pseudo-second-order kinetic model is a good fit to the adsorption of MG. It also means that the adsorption process might be of a chemical nature ascribed to π orbital hybridization. In addition, adsorption on the external surface of oxygen-containing groups can form electronic interactions for rapidly capturing MG molecules.

3.5 Adsorption mechanism

GO/Fe_3O_4 has a lot of oxygen-containing groups with negative charge that can be regarded as Lewis bases,[51] which helps to improve the affinity between cationic MG and GO/Fe_3O_4. In order to further confirm the adsorption mechanism of electronic interaction, three anionic dyes (Methyl Red, Acid Fuchsin and Aniline Blue) and three cationic dyes (Neutral Red, Basic Fuchsin and Crystal Violet) were selected as adsorbates onto the same amount of GO and GO/Fe_3O_4, respectively. Experimental conditions: dye concentration was 20 mg L^{-1}, dosage was 10 mg, pH was 7.08, contact time was 200 min, and temperature was 289 K. The results showed that adsorbance of anionic dyes onto both GO and GO/Fe_3O_4 (Fig. 5A) was much lower than that of cationic dyes (Fig. 5B). It was demonstrated that GO/Fe_3O_4 was capable of adsorbing various types of cationic dyes *via* electrostatic interaction. Dyes adsorbed onto binary GO/Fe_3O_4 were absolutely enhanced compared to unitary GO, because of the increased surface areas in the heterogeneous structure.[52] Furthermore, GO/Fe_3O_4 was also available to adsorb anionic dyes slightly, which could be due to another adsorption mechanism such as interactions of π orbit electrons.[33,53]

In order to further confirm both adsorption forces, the functional groups on the spent GO/Fe_3O_4 after adsorption are shown in Fig. 2D. The band of O–H stretching vibration at 3430 cm^{-1} was narrower after adsorption of MG. The peak at 1225 cm^{-1} disappeared after adsorption, which was attributed to oxygen-containing functional groups, while the peaks at 1080 cm^{-1} and 980 cm^{-1} could be explained by the formation of new chemical bonds, *i.e.* C–OH and π–π conjugations.[54] As for MG, the C–N bending and stretching vibrations[55] were observed at 1120 cm^{-1} and 615 cm^{-1}, but both vibrations decreased and shifted significantly after adsorption, indicating the attachment of $-N^+$ to GO/Fe_3O_4 by electrostatic force. Considering the UV-vis spectrum assay, the spectral peaks of MG solution integrally decreased with an increased dosage of GO/Fe_3O_4 without a shift in spectral peaks or other peaks emerging. This suggests that the initial MG would be adsorbed due to electronic interaction and π–π conjugations, and the final concentration of MG would be reduced.

3.6 Desorption and re-adsorption of environmentally-friendly GO/Fe_3O_4

The experiments of MG desorbed from the spent GO/Fe_3O_4 were performed in a warmed water bath from 60 °C to 90 °C desorption temperature. As shown in Fig. 6, elevated temperatures higher than 80 °C resulted in good desorption. The re-adsorption capacity (58.0 mg g^{-1}) at 80 °C is almost the same as the initial adsorption capacity (59.0 mg g^{-1}), indicating that the adsorption of MG onto GO/Fe_3O_4 follows the reversible adsorption of the Freundlich model. Reversible adsorption means GO/Fe_3O_4 can be sustainably utilized as an environmentally-friendly material.

The recoverability and stability of the adsorbent are crucial to the development of advanced treatment technology. After the

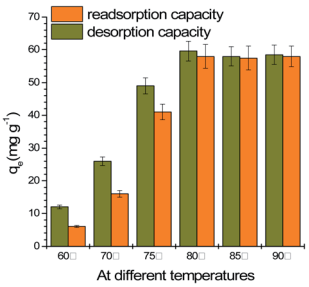

Fig. 6 Desorption and re-adsorption capacities in a water bath at elevated temperatures (MG concentration = 10, 20, 30, 40, 50 mg L^{-1}, dosage = 10 mg, pH = 7.08, time = 200 min).

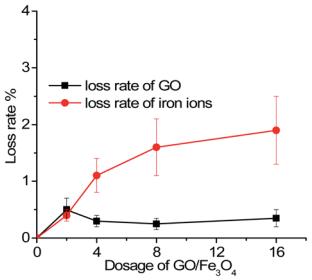

Fig. 7 The mean loss rate of GO and iron ions *vs.* different dosages of GO/Fe_3O_4 (MG concentration = 9 mg L^{-1}, temperature = 298 K, pH = 7.08, time = 200 min).

re-adsorption of the spent GO/Fe_3O_4, concentrations of the residual iron ions and GO in solutions were detected. Based on the law of conservation of mass, the lost weight was calculated and compared with the total mass of the adsorbent, as can be seen in Fig. 7. It was demonstrated that the mean loss rate of GO was less than 0.5% and that of iron ions was less than 2%.

4. Conclusion

In this work, GO/Fe_3O_4 shows heterogeneous phases with a lot of oxygen-containing groups and a large specific surface area of 132.2 m^2 g^{-1}. The mass ratio of GO in the adsorbent and the pH value in solution were determining factors for efficient MG removal, reaching an adsorption capacity of 59 mg g^{-1} at pH 7 within 200 min. It is supposed that the electrostatic interaction and π–π conjugations contribute the attractive force to capture MG molecules. An almost completely reversible adsorption/desorption procedure suggests that GO/Fe_3O_4 is a promising adsorbent for the circular removal of contaminants. The advantages of its stability, reversibility and recoverability even make it possible to synergize with plants, microorganisms or animals for ecological remediation.

Conflicts of interest

There are no conflicts to declare.

Acknowledgements

This work was funded by National Nature Science Foundation of China (No. 20975001) and Collaborative Innovation Center of Recovery and Reconstruction of Degraded Ecosystem in Wanjiang Basin Co-founded by Anhui Province and Ministry of Education (GXXT-2020-075).

References

1 S. Srivastava, R. Sinha and D. Roy, *Aquat. Toxicol.*, 2004, **66**, 319–329.
2 F. Ding, X. N. Li, J. X. Diao, Y. Sun, L. Zhang, L. Ma, X. L. Yang, L. Zhang and Y. Sun, *Ecotoxicol. Environ. Saf.*, 2012, **78**, 41–49.
3 B. H. Hameed and M. I. El-Khaiary, *J. Hazard. Mater.*, 2008, **154**, 237–244.
4 D. Robati, M. Rajabi, O. Moradi, F. Najafi, I. Tyagi, S. Agarwal and V. K. Gupta, *J. Mol. Liq.*, 2016, **214**, 259–263.
5 N. Bilandžić, I. Varenina, B. S. Kolanović, D. Oraić and S. Zrnčić, *Food Control*, 2012, **26**, 393–396.
6 A. ZakariyahJamiu, A. TawfikSaleh and A. ShaikhAli, *RSC Adv.*, 2015, 42222–42232.
7 M. Tuzen, T. A. Saleh and A. Sarı, *Chem. Eng. Res. Des.*, 2020, **159**, 353–361.
8 T. A. Saleh, M. Tuzen and A. Sarı, *Chem. Eng. Res. Des.*, 2016, **117**, 218–227.
9 R. K. Upadhyay, M. Sharma, D. K. Singh, S. S. Amritphale and N. Chandra, *Sep. Purif. Technol.*, 2012, **88**, 39–45.
10 A. M. Aljeboree, A. F. Alkaim, A. Loay and H. M. Algburi, *J. Global Pharma Technol.*, 2019, **11**, 138–143.
11 V. K. Gupta, R. Jain, A. Mittal, T. A. Saleh, A. Nayak, S. Agarwal and S. Sikarwar, *Mater. Sci. Eng., C*, 2012, **32**, 12–17.
12 Y. Hu, Y. Li, J. He, T. Liu, K. Zhang, X. Huang, L. Kong and J. Liu, *J. Environ. Manage.*, 2018, **226**, 256–263.
13 A. N. Kagalkar, M. U. Jadhav, V. A. Bapat and S. P. Govindwar, *Bioresour. Technol.*, 2011, **102**, 10312–10318.
14 V. K. Gupta, I. Ali, T. A. Saleh and S. Agarwal, *RSC Adv.*, 2012, **2**, 6380–6388.
15 Y. C. Lee, E. J. Kim, J. W. Yang and H. J. Shin, *J. Hazard. Mater.*, 2011, **192**, 62–70.
16 G. Wang, G. Li, Y. Huan, C. Hao and W. Chen, *Chemosphere*, 2020, **261**, 127736.
17 Z. Bekçi, C. Özveri, Y. Seki and K. Yurdakoç, *J. Hazard. Mater.*, 2008, **154**, 254–261.
18 Z. Cui, J. Liu, H. Gao, Y. Xue, J. Hao, R. Zhang, B. Ji and J. Chen, *Phys. Chem. Chem. Phys.*, 2019, **21**, 13721–13729.
19 M. AmaniAlansi, Z. WaedAlkayali, H. MahaAl-qunaibit, F. TalalQahtan and A. TawfikSaleh, *RSC Adv.*, 2015, **5**, 71441–71448.
20 J. Yu, L. Zhang and B. Liu, *Int. J. Environ. Res. Public Health*, 2019, **16**, 3297.
21 M. Choudhary, R. Kumar and S. Neogi, *J. Hazard. Mater.*, 2020, **392**(15), 122441.
22 N. Shah, T. Rehan, X. Li, H. Tetik, G. Yang, K. Zhao and D. Lin, *RSC Adv.*, 2021, **11**, 7187–7204.
23 J. Y. Lim, N. M. Mubarak, E. C. Abdullah, S. Nizamuddin, M. Khalid and Inamuddin, *J. Ind. Eng. Chem.*, 2018, **66**, 29–44.
24 Y. Li, P. Zhang, Q. Du, X. Peng, T. Liu, Z. Wang, Y. Xia, W. Zhang, K. Wang, H. Zhu and D. Wu, *J. Colloid Interface Sci.*, 2011, **363**, 348–354.
25 T. Liu, Y. Li, Q. Du, J. Sun, Y. Jiao, G. Yang, Z. Wang, Y. Xia, W. Zhang, K. Wang, H. Zhu and D. Wu, *Colloids Surf., B*, 2012, **90**, 197–203.
26 O. Suárez-Iglesias, S. Collado, P. Oulego and M. Díaz, *Chem. Eng. J.*, 2017, **313**, 121–135.
27 F. Najafi, *Int. Nano Lett.*, 2015, **5**, 171–178.
28 Y. Zhao, D. Zhao, C. Chen and X. Wang, *J. Colloid Interface Sci.*, 2013, **405**, 211–217.

29 H. C. Vu, A. D. Dwivedi, T. T. Le, S. H. Seo, E. J. Kim and Y. S. Chang, *Chem. Eng. J.*, 2017, **307**, 220–229.
30 Shagufta, R. Dhar, B. S. Kim, A. Alblooshi and I. Ahmad, *Int. J. Eng. Technol.*, 2018, **7**, 3007–3013.
31 K. Gupta and O. P. Khatri, *J. Colloid Interface Sci.*, 2017, **501**, 11–21.
32 P. Russo, L. D'Urso, A. Hu, N. Zhou and G. Compagnini, *Appl. Surf. Sci.*, 2015, **348**, 85–91.
33 J. Xu, L. Wang and Y. Zhu, *Langmuir*, 2012, **28**, 8418–8425.
34 M. R. Islam, M. Ferdous, M. I. Sujan, X. Mao, H. Zeng and M. S. Azam, *J. Colloid Interface Sci.*, 2020, **562**, 52–62.
35 J. Zhang, M. Liu, Z. Liu, T. Yang, Q. He, K. Yang and H. Wang, *J. Sol-Gel Sci. Technol.*, 2017, **82**, 424–431.
36 A. Mishra, *Vacuum*, 2018, **157**, 524–529.
37 Y. Xu, J. Jin, X. Li, C. Song, H. Meng and X. Zhang, *Desalin. Water Treat.*, 2016, **57**, 25216–25225.
38 W. S. Hummers and R. E. Offeman, *J. Am. Chem. Soc.*, 1958, **80**, 1339.
39 J. F. Wu, M. Q. Xu and G. C. Zhao, *Electrochem. Commun.*, 2010, **12**, 175–177.
40 M. H. Kahsay, N. Belachew, A. Tadesse and K. Basavaiah, *RSC Adv.*, 2020, **10**, 34916–34927.
41 G. Fadillah, W. P. Wicaksono, I. Fatimah and T. A. Saleh, *Microchem. J.*, 2020, **159**, 105353.
42 H. Zhang and X. Hu, *J. Environ. Chem. Eng.*, 2017, **5**, 3348–3353.
43 A. M. Alansi, T. F. Qahtan and T. A. Saleh, *Adv. Mater. Interfaces*, 2021, **8**, 1–10.
44 S. Chong, G. Zhang, H. Tian and H. Zhao, *J. Environ. Sci.*, 2016, **44**, 148–157.
45 Y. Liu, L. Xu, J. Liu, X. Liu, C. Chen, G. Li and Y. Meng, *Chem. Eng. J.*, 2016, **285**, 698–708.
46 T. A. Saleh, *Appl. Surf. Sci.*, 2011, **257**, 7746–7751.
47 T. Paszko, *Sci. Total Environ.*, 2012, **435–436**, 222–229.
48 T. W. Weber and R. K. Chakravorti, *AIChE J.*, 1974, **20**, 228–238.
49 I. Langmuir, *J. Am. Chem. Soc.*, 1918, **40**, 1361–1403.
50 M. Ertaş, B. Acemioğlu, M. H. Alma and M. Usta, *J. Hazard. Mater.*, 2010, **183**, 421–427.
51 X. Zhao, X. Xu, J. Teng, N. Zhou, Z. Zhou, X. Jiang and F. Jiao, *Ecotoxicol. Environ. Saf.*, 2019, **176**, 11–19.
52 J. Li, J. Tao, C. Ma, J. Yang, T. Gu and J. Liu, *RSC Adv.*, 2020, **10**, 42038–42053.
53 K. C. Lai, L. Y. Lee, B. Yan, Z. Hiew, S. Thangalazhy-gopakumar and S. Gan, *J. Environ. Sci.*, 2018, **79**, 174–199.
54 Z. Fang, Y. Hu, X. Wu, Y. Qin and J. Cheng, *Chem. Eng. J.*, 2018, **334**, 948–956.
55 Z. Shi, C. Xu, H. Guan, L. Li, L. Fan, Y. Wang, L. Liu, Q. Meng and R. Zhang, *Colloids Surf., A*, 2018, **539**, 382–390.